

Data-Driven Spectral Submanifold Reduction for Nonlinear Optimal Control of Soft Robots

John Irvin Alora¹, Mattia Cenedese², Edward Schmerling¹, George Haller², Marco Pavone¹

Abstract—Modeling and control of continuum soft robots remains a challenging task due to their inherent nonlinearities and high degrees of freedom. These complexities hinder the construction of high-fidelity models appropriate for real-time control. While various model and learning-based approaches have been proposed to address these challenges, they lack generalizability and rarely preserve the structure of the dynamics. In this work, we propose a new, data-driven approach for extracting control-oriented models on invariant manifolds from data. We overcome the issues outlined above and demonstrate our superior performance of Spectral Submanifold Reduction (SSMR) *vis-à-vis* the state of the art.

I. INTRODUCTION

Soft continuum robots promise to revolutionize the field of robotics due to their versatility over their rigid-body counterparts. Their compliance and elasticity make them well-suited to operate in delicate, geometrically constrained environments, which enable them to play crucial roles in settings where safe human-robot interaction is paramount. These advantages, however, also pose significant practical challenges for the modeling and control of these robots.

Statement of Contributions: Motivated by recent developments in *Spectral Submanifold* (SSM) theory [1] and its successful application to data-driven predictions of nonlinearizable phenomena [2], we propose a new, data-driven *Spectral Submanifold Reduction* (SSMR) approach for the modeling and control of soft robots. Specifically, we achieve real-time control of a cable-actuated soft robot for trajectory following tasks using low-dimensional, control-oriented models learned on an SSM in a nonlinear, model predictive control (MPC) framework.

Our contributions are threefold:

- (i) We present, for the first time, a data-driven approach for learning soft robot dynamics on invariant manifolds. By fitting control-oriented models to structurally-invariant sets in the phase space, we overcome common drawbacks associated with data-driven approaches such as lack of generalizability, high-data requirement, and sensitivity to noise.
- (ii) While fully data-driven, our approach nevertheless automatically enforces self-consistent nonlinear dynamics

J.A. is supported by the Secretary of the Air Force STEM Ph.D. Fellowship.

¹Department of Aeronautics and Astronautics, Stanford University, Stanford, CA, 94305, USA {jjalora, schmrlng, pavone}@stanford.edu

²Institute of Mechanical Systems, ETH Zurich, 8092 Zurich, Switzerland {mattiacc, georgehaller}@ethz.ch

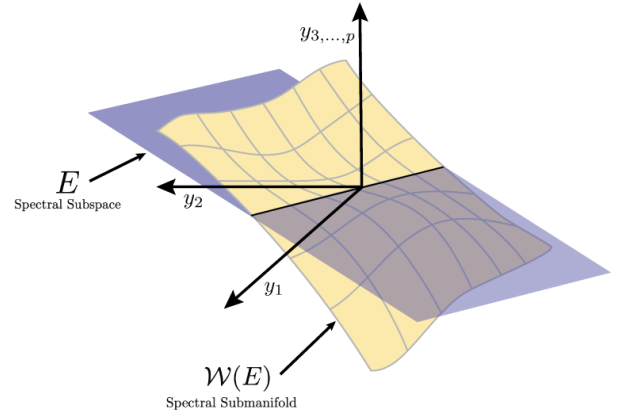


Fig. 1. An SSM is a low-dimensional attracting invariant manifold in the robot's phase space. Specifically, SSMs are the smoothest invariant manifolds that nonlinearly extend the eigenspace of the linear part of a system at an equilibrium point. These nonlinear continuations can capture highly nonlinear behaviors that characterize soft robot deformations and can be approximated with arbitrarily high accuracy without increasing the dimension of the SSM.

for the robot without relying on the governing equations. This structure results in low-dimensional models that are amenable to real-time control schemes.

- (iii) We validate SSMR on simulations of a high-dimensional soft robot and show that it outperforms the state-of-the-art methods in both trajectory tracking performance and computational efficiency.

Related Work: A popular approach in the modeling of soft robots is to use simplified assumptions that approximate the robot's behavior. Examples of this approach include a Cosserot rod model [3], piecewise-constant curvature models [4], and lumped-mass models [5]. Unfortunately, these methods are only accurate for specific types of geometries and their low fidelity precludes their use in more challenging control tasks.

Another approach, the projection-based reduction of Finite Element Models (FEM), has seen some success in various settings. For example, [6], [7], and [8] showed successful application of this type of model reduction for control on linearized FEM models. The authors in [9] apply proper orthogonal decomposition (POD) in a piecewise-affine fashion by reducing linear approximations of a high-fidelity model. They then evaluate the nonlinearities through interpolation of the linear approximations and apply an MPC framework to control a soft robot. The work in [10] considers a more sophisticated model reduction approach using *hyper-reduction*

to approximate the nonlinear terms, but applies it only in a simple inverse-kinematic control scheme.

A common limitation of these projection-based techniques is that the accuracy of the low-dimensional surrogate depends on the choice and size of the subspace. Additionally, the process of extracting control-oriented models from FEM code is an encumbering and code-intrusive process. These drawbacks make it challenging for control practitioners to test and implement these approaches in the growing field of soft robot control.

To overcome these challenges, there has been increasing interest in using machine learning techniques to construct data-driven models of soft robots. While much of the literature has been focused on using neural networks (NN) to learn approximations of the dynamics of these systems for control [11], finite-dimensional, data-driven approximations of Koopman operators were shown to outperform standard NN models for predicting soft robot dynamics in [12]. Since observed dynamics under the Koopman Operator are linear, the approach lends itself to established control techniques such as MPC, as shown in [13]. Although this approach is conceptually appealing, finding physically realizable observables that span a Koopman eigenspace (*e.g.*, which include the original state variables) has technically zero probability [14]. Additionally, achieving good control performance in closed-loop requires a significant tuning of various hyperparameters.

Organization: We begin in Section II by considering the soft robot dynamics as a high-dimensional mechanical system and pose the associated nonlinear optimal control problem. In Section III, we summarize relevant results from SSM theory and outline the data-driven procedure for learning control dynamics on SSMs. We then discuss our proposed control procedure in Section IV and present simulation results in Section V.

II. PROBLEM FORMULATION

A. Soft Robot Mechanical System

We consider control-affine soft robots modeled as mechanical systems with $\mathcal{N} \in \mathbb{Z}_+$ degrees of freedom (DOF). Such systems are of the form

$$\mathbf{M}\ddot{\mathbf{q}}(t) + \mathbf{C}\dot{\mathbf{q}}(t) + \mathbf{K}\mathbf{q}(t) + \mathbf{F}_{\text{int}}(\mathbf{q}(t), \dot{\mathbf{q}}(t)) = \mathbf{H}\mathbf{u}(t), \quad (1)$$

where $\mathbf{q}(t) \in \mathbb{R}^{\mathcal{N}}$ is the vector of generalized coordinates, $\mathbf{M} \in \mathbb{R}^{\mathcal{N} \times \mathcal{N}}$ is the mass matrix, $\mathbf{C} \in \mathbb{R}^{\mathcal{N} \times \mathcal{N}}$ represents the damping matrix, $\mathbf{K} \in \mathbb{R}^{\mathcal{N} \times \mathcal{N}}$ is the stiffness matrix, and $\mathbf{F}_{\text{int}}(\mathbf{q}, \dot{\mathbf{q}}) \in \mathbb{R}^{\mathcal{N}}$ represents the internal nonlinear forces. Also $\mathbf{u}(t) \in \mathbb{R}^m$ is the vector of inputs and $\mathbf{H} \in \mathbb{R}^{\mathcal{N} \times m}$ represents the linear mapping of actuation forces from their point of application to the configuration space. In the continuum limit (*i.e.*, $\mathcal{N} \rightarrow \infty$), Equation (1) converges to the exact model [15].

The second-order formulation in Equation (1) can be rewritten in first-order form with the state vector $\mathbf{x}^f(t) = [\mathbf{q}(t), \dot{\mathbf{q}}(t)]^\top \in \mathbb{R}^{n_f}$ as

$$\dot{\mathbf{x}}^f(t) = \mathbf{A}\mathbf{x}^f(t) + \mathbf{f}_{\text{nl}}(\mathbf{x}^f(t)) + \epsilon\mathbf{B}\mathbf{u}(t), \quad (2)$$

where $n_f = 2\mathcal{N}$, $\mathbf{A} \in \mathbb{R}^{n_f \times n_f}$ is assumed to be negative-definite (*i.e.*, the origin is an asymptotically stable fixed point) and $\mathbf{B} \in \mathbb{R}^{n_f \times m}$ represents the linear control matrix. The nonlinear term $\mathbf{f}_{\text{nl}} : \mathbb{R}^{n_f} \rightarrow \mathbb{R}^{n_f}$ belongs to the class of analytic functions, $\mathbf{x}^f(t) : \mathbb{R}^{n_f}$ represents the full state vector, and the parameter $0 < \epsilon \ll 1$ makes explicit our assumption that the control inputs are moderate.

B. Constrained Optimal Control Problem

We now pose the problem of controlling soft robots to follow arbitrary and dynamic trajectories in the vicinity of the origin. Consider the following continuous-time, optimal control problem (OCP) with quadratic cost and polytopic constraints in states and control:

$$\begin{aligned} & \underset{\mathbf{u}(\cdot)}{\text{minimize}} \quad \|\delta\mathbf{z}(t_f)\|_{\mathbf{Q}_f} + \int_{t_0}^{t_f} \left(\|\delta\mathbf{z}(t)\|_{\mathbf{Q}} + \|\mathbf{u}(t)\|_{\mathbf{R}} \right) dt, \\ & \text{subject to} \quad \mathbf{x}^f(0) = \mathbf{g}(\mathbf{z}(0)), \\ & \quad \dot{\mathbf{x}}^f(t) = \mathbf{A}\mathbf{x}^f(t) + \mathbf{f}_{\text{nl}}(\mathbf{x}^f(t)) + \epsilon\mathbf{B}\mathbf{u}(t), \\ & \quad \mathbf{y}(t) = \mathbf{h}(\mathbf{x}^f(t)), \quad \mathbf{z}(t) = \mathbf{C}\mathbf{y}(t), \\ & \quad \mathbf{u} \in \mathcal{U}, \quad \mathbf{z} \in \mathcal{Z}. \end{aligned} \quad (3)$$

Here, $\delta\mathbf{z}(t) = \mathbf{z}(t) - \bar{\mathbf{z}}(t)$ is the tracking difference between the performance variable, $\mathbf{z}(t) \in \mathbb{R}^o$ and the desired trajectory $\bar{\mathbf{z}}(t) \in \mathbb{R}^o$. The observed state is denoted as $\mathbf{y}(t) \in \mathbb{R}^p$ and $[t_0, t_f]$ represents the time horizon. $\mathbf{Q}, \mathbf{Q}_f \in \mathbb{R}^{o \times o}$ are positive semi-definite matrices which represent the stage and terminal costs, respectively, over the performance variables, while \mathbf{R} is a positive-definite matrix representing the cost on controls. The functions $\mathbf{g} : \mathbb{R}^o \rightarrow \mathbb{R}^{n_f}$ and $\mathbf{h} : \mathbb{R}^{n_f} \rightarrow \mathbb{R}^p$ map the performance variable to the full state and the full state to the observed state, respectively, while $\mathbf{C} \in \mathbb{R}^{o \times p}$ is a selection matrix of states that we observe. Lastly, the constraint sets are defined as $\mathcal{U} := \{\mathbf{u}(t) \in \mathbb{R}^m : \mathbf{M}_u\mathbf{u}(t) \leq \mathbf{b}_u\}$ and $\mathcal{Z} := \{\mathbf{z} \in \mathbb{R}^o : \mathbf{M}_z\mathbf{z}(t) \leq \mathbf{b}_z\}$ with $\mathbf{M}_u \in \mathbb{R}^{n_u \times m}$ and $\mathbf{M}_z \in \mathbb{R}^{n_z \times o}$, where n_u and n_z represent the number of constraints in the inputs and the observed states, respectively.

Accurate approximations of the exact model typically generate high-dimensional dynamical systems (*i.e.*, $n_f \gg 1$). Thus, dimensionality becomes a bottleneck and it is intractable to solve the OCP (3) in an online fashion.

III. DATA-DRIVEN MODELING OF SOFT ROBOT DYNAMICS

In this section, we describe our data-driven SSMR procedure to construct controlled, predictive models of soft robots from data. Our approach entails learning low-dimensional models directly as the reduced dynamics on attracting, low-dimensional invariant manifolds that generically exist in dissipative physical systems.

A. Reduced Order Models on SSMs

Recent results in nonlinear dynamics establish the existence of unique, smoothest invariant structures in the phase space of Equation (2) [1]. These SSMs are nonlinear continuations of the spectral subspaces of the linearization of

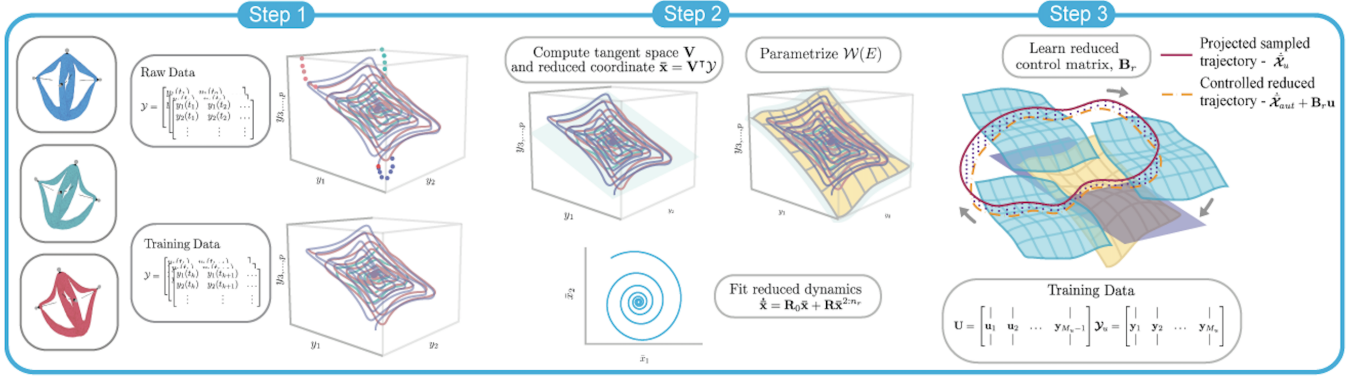


Fig. 2. Three-step procedure to learn control-oriented dynamics on the SSM. Step 1 details the data collection procedure whereby we displace the robot across various parts of its workspace and collect decaying trajectories. We then form our training data by truncating the dataset to approximate trajectories that are on or near the manifold. Step 2 computes the SSM parameterization and autonomous dynamics while step 3 regresses the control matrix which best explains how the autonomous SSM is translated under the influence of control. The “Diamond” soft robot is shown in its various displaced configurations on the far left.

Equation (2). Formally, let us define E as the direct sum of an arbitrary collections of eigenspaces of \mathbf{A} i.e.,

$$E := E_{j_1} \oplus E_{j_2} \oplus \dots \oplus E_{j_n}.$$

where E_{j_k} denotes the real eigenspace corresponding to an eigenvalue λ_{j_k} of \mathbf{A} . The SSM corresponding to E in the autonomous part of Equation (2) is then defined as follows.

Definition 1: An autonomous SSM, $\mathcal{W}(E)$, corresponding to a spectral subspace E of the operator \mathbf{A} is an invariant manifold of the autonomous part of the nonlinear system (2) such that

- 1) $\mathcal{W}(E)$ is tangent to E at the origin and has the same dimension as E ,
- 2) $\mathcal{W}(E)$ is strictly smoother than any other invariant manifold satisfying condition 1 above.

A slow SSM is associated with a non-resonant spectral subspace containing the slowest decaying eigenvectors of the linearized system. Technical details on existence of SSMs are given in [1], [2]. Slow SSMs are ideal candidates for model reduction as nearby full system trajectories become exponentially attracted towards these manifolds and synchronize with the slow dynamics on the SSM.

In general, since we seldom have access to the full state \mathbf{x}^f , we must construct the SSM and the reduced dynamics of our system in the space of observed states such that $p \geq 2n+1$ by the Takens embedding theorem [2]. In case \mathbf{y} does not satisfy this condition, we use time-delay embeddings of \mathbf{y} to embed $\mathcal{W}(E)$ in a space with appropriate dimension, p .

To describe the geometry of $\mathcal{W}(E)$, we seek a pair $\mathbf{w}(\mathbf{x})$, $\mathbf{w}(\mathbf{y})$ of smooth, invertible functions where $\mathbf{y} = \mathbf{w}(\mathbf{x})$ uniquely maps the reduced state on the SSM to the observed state and $\mathbf{x} = \mathbf{v}(\mathbf{y})$ maps the observed state to the reduced coordinates, where $\mathbf{x} \in \mathbb{R}^n$ is the reduced state. By definition of the invariance and tangency properties of the SSM, the two maps that parameterize $\mathcal{W}(E)$ must satisfy the invertibility

relations, $\mathbf{y} = (\mathbf{w} \circ \mathbf{v})(\mathbf{y})$ and $\mathbf{x} = (\mathbf{v} \circ \mathbf{w})(\mathbf{x})$ such that

$$\begin{aligned} \mathbf{x} &= \mathbf{v}(\mathbf{y}) := \mathbf{V}^T \mathbf{y}, \\ \mathbf{y} &= \mathbf{w}(\mathbf{x}) := \mathbf{W}_0 \mathbf{x} + \mathbf{W} \mathbf{x}^{2:n_w}, \end{aligned} \quad (4)$$

where $\mathbf{x}^{2:n_w}$ is the family of all monomials from order 2 to n_w , and n_w is the desired order of the polynomial expansion for the SSM. Also, the columns of $\mathbf{V} \in \mathbb{R}^{n_f \times n}$ span the spectral subspace of E and \mathbf{W}_0, \mathbf{W} represent coefficient matrices of the SSM parameterization. In addition, the reduced dynamics on $\mathcal{W}(E)$ is represented by

$$\dot{\mathbf{x}}_{\text{aut}} = \mathbf{r}_{\text{aut}}(\mathbf{x}) := \mathbf{R}_0 \mathbf{x} + \mathbf{R} \mathbf{x}^{2:n_r}, \quad (5)$$

where $\mathbf{r}_{\text{aut}} : \mathbb{R}^n \rightarrow \mathbb{R}^n$ is the autonomous reduced dynamics on the SSM; \mathbf{R}_0 and \mathbf{R} represent the corresponding coefficient matrices. Since $\mathcal{W}(E)$ is locally a graph over the spectral subspace E [2], we can identify the full state trajectory of System (2) on $\mathcal{W}(E)$ described by Equation (5). Figure 1 gives an intuitive depiction of this concept.

We seek to learn the SSM-reduced for control and construct mappings that describe the trajectory of our observed states on SSMs. Our three-step SSMR procedure involves: (1) collecting trajectories at or near the SSM. (2) learning the SSM geometry and the reduced dynamics in Equation (5), followed by 3) learning a linear control matrix that describes the effect of the controls in the reduced coordinates. Figure 2 summarizes the complete data-driven SSMR approach.

B. Learning Autonomous Dynamics on SSMs

To learn the geometry and reduced dynamics on the SSM, the training data should involve only trajectories that are near the SSM. Thus, we obtain training data snapshots by displacing the robot along various directions in its workspace then collect the observed state trajectory as it decays to its equilibrium position. In other words, we form an augmented matrix of M_y (possibly time-delayed) decay datasets $\mathcal{Y} = [\mathcal{Y}_1, \dots, \mathcal{Y}_{M_y}]$, as shown in Figure 2. We remove initial transients converging to the SSM in our datasets \mathcal{Y} by truncating the first few states in the decay trajectories [16].

To start, we first compute \mathbf{V} by finding the n dominant modes of Equation (2). To do this we carry out principle component analysis (PCA) on the trajectory dataset \mathcal{Y} and pick the n leading directions that capture a majority of the variance in the data. Indeed, for systems that do not feature strong nonlinearities, PCA is able to obtain a close estimate for the spectral subspace E to which the SSM is tangent [17].

Now, we can learn the parameterization of $\mathcal{W}(E)$ (i.e., learn the map \mathbf{w}) by finding \mathbf{W} and \mathbf{W}_0 via polynomial regression

$$(\mathbf{W}_0^*, \mathbf{W}^*) = \arg \min_{\mathbf{W}_0, \mathbf{W}} \|\mathcal{Y} - \mathbf{W}_0 \mathbf{V}^\top \mathcal{Y} - \mathbf{W} (\mathbf{V}^\top \mathcal{Y})^{2:n_w}\|_F^2. \quad (6)$$

In a similar fashion, we can compute the polynomial form of the reduced dynamics in Equation (9) by finding the coefficients \mathbf{R}_0 and \mathbf{R} via the regression

$$(\mathbf{R}_0^*, \mathbf{R}^*) = \arg \min_{\mathbf{R}_0, \mathbf{R}} \|\dot{\mathcal{X}} - \mathbf{R}_0 \mathcal{X} - \mathbf{R} \mathcal{X}^{2:n_r}\|_F^2, \quad (7)$$

where $\mathcal{X} = \mathbf{V}^\top \mathcal{Y}$. The time derivative in Equation (7) can be computed using standard finite difference schemes if the sampling time of \mathcal{X} is much smaller than the Nyquist sampling time of the fastest mode in the SSM dynamics. Otherwise, we can also compute a discrete-time alternative to Equation (9) using a similar procedure through simple shifting operations on the dataset as in [18].

This approach is suitable for both from numerical and experimental data. For the former, we can choose $\mathbf{y}(t) = \mathbf{x}^f(t)$ and let the dataset \mathcal{Y} consist of full state information during decay. We implement this procedure using a modified version of *SSMLearn* [2].

C. Learning the Control Matrix

Once the reduced autonomous dynamics on $\mathcal{W}(E)$ is known, we seek to learn the contribution of control in the reduced coordinates. Our goal is to find the best linear control matrix $\mathbf{B}_r \in \mathbb{R}^{n \times m}$ which best explains the difference between the controlled dynamics and our model of the autonomous dynamics. We explore the actuation space of the robot by randomly sampling a sequence of inputs, \mathbf{U} , and recording the corresponding (possibly time-delayed) observed state trajectory \mathcal{Y}_u , as depicted in Figure 2

We then project the observed states down to the reduced coordinates and form the reduced state matrix $\mathcal{X}_u = \mathbf{V}^\top \mathcal{Y}_u$. Additionally, we evaluate our model of the autonomous dynamics and form the matrix $\dot{\mathcal{X}}_{\text{aut}} = \mathbf{r}_{\text{aut}}(\mathcal{X}_u)$. Learning the (continuous-time) control matrix from data amounts to solving the minimization problem

$$\mathbf{B}_r^* = \arg \min_{\mathbf{B}_r} \|\dot{\mathcal{X}}_u - \dot{\mathcal{X}}_{\text{aut}} - \mathbf{B}_r \mathbf{U}\|_F^2, \quad (8)$$

where $\dot{\mathcal{X}}_u$ is computed by finite differencing \mathcal{X}_u . Our learned, low-dimensional control dynamics is thus,

$$\dot{\mathbf{x}} = \mathbf{r}(\mathbf{x}, \mathbf{u}) := \mathbf{R}_0 \mathbf{x} + \mathbf{R} \mathbf{x}^{2:n_r} + \epsilon \mathbf{B}_r \mathbf{u}. \quad (9)$$

From a theoretical point of view, results on the existence of non-autonomous SSMs subject to quasi-periodic forcing

were established in [1]. Since quasi-periodic signals over a finite time interval are dense in the space of continuous signals over the same interval, we can interpret the trajectory of the system under control input as lying approximately on a time-varying, invariant manifold that is ϵ -perturbed from $\mathcal{W}(E)$.

In general, the introduction of control causes $\mathcal{W}(E)$ to lose its invariance. Intuitively, though, we expect that the trajectories will remain within a small neighborhood of $\mathcal{W}(E)$ since the effect of our control input is moderate compared to the system dynamics. Thus, we interpret this step as regressing a linear matrix that optimally translates the autonomous SSM under control inputs to be as close as possible to off-SSM trajectories.

IV. SSM-BASED NONLINEAR MPC

A. Reduced Order Optimal Control Problem

Learning the parameterization of $\mathcal{W}(E)$ enables us to learn the intrinsic physics of our system, leading to low-dimensional and accurate reduced models with $n \ll n_f$. This allows us to approximate the OCP in (3) by posing an optimization problem with respect to the dynamics on the SSM as follows

$$\begin{aligned} & \underset{\mathbf{u}(\cdot)}{\text{minimize}} \quad \|\delta \mathbf{z}(t_f)\|_{\mathbf{Q}_f}^2 + \sum_{k=1}^{N-1} \left(\|\delta \mathbf{z}(t_k)\|_{\mathbf{Q}}^2 + \|\mathbf{u}(t_k)\|_{\mathbf{R}}^2 \right) \\ & \text{subject to} \quad \mathbf{x}(0) = \mathbf{V}^\top (\mathbf{y}(0) - \mathbf{y}_{\text{eq}}), \\ & \quad \mathbf{x}(t) = \mathbf{r}(\mathbf{x}(t)) + \epsilon \mathbf{B}_r \mathbf{u}(t), \\ & \quad \mathbf{z}(t) = \mathbf{C} \mathbf{w}(\mathbf{x}(t)) + \mathbf{z}_{\text{eq}}, \\ & \quad \mathbf{z}(t) \in \mathcal{Z}, \quad \mathbf{u}(t) \in \mathcal{U}, \end{aligned} \quad (10)$$

where $\mathbf{z}_{\text{eq}} \in \mathbb{R}^p$ and $\mathbf{y}_{\text{eq}} \in \mathbb{R}^p$ are the performance and observed states at equilibrium. To solve the approximate OCP (10) numerically, we discretize the continuous-time system and employ standard numerical optimization to obtain the solution.

The resulting problem is, however, a nonconvex optimization problem, due to the nonlinearities in the reduced dynamics and the mapping to the performance variables. Nonconvex optimization typically has high computational complexity and no guarantee for the existence of a certifiable solution. These limitations preclude the use of generic nonlinear programs for solving the approximate OCP (10) for real-time and safety-critical applications.

B. Convex Formulation for Real-Time Control

Convex optimization allows us to leverage fast, iterative algorithms with polynomial-time complexity [19] to efficiently and reliably approximate a solution to (10). We use sequential convex programming (SCP) to transform the nonlinear equality constraints into a sequence of linear equality constraints. The key idea is then to iteratively re-linearize the dynamics around a nominal trajectory and solve a convex approximation near this trajectory until convergence to a local optimum of the continuous-time OCP (10) is observed.

To be precise, suppose we have some nominal trajectory of states and controls $(\mathbf{x}^j, \mathbf{u}^j) = (\{\mathbf{x}_k^j\}_{k=1}^N, \{\mathbf{u}_k^j\}_{k=1}^{N-1})$ at the j -th

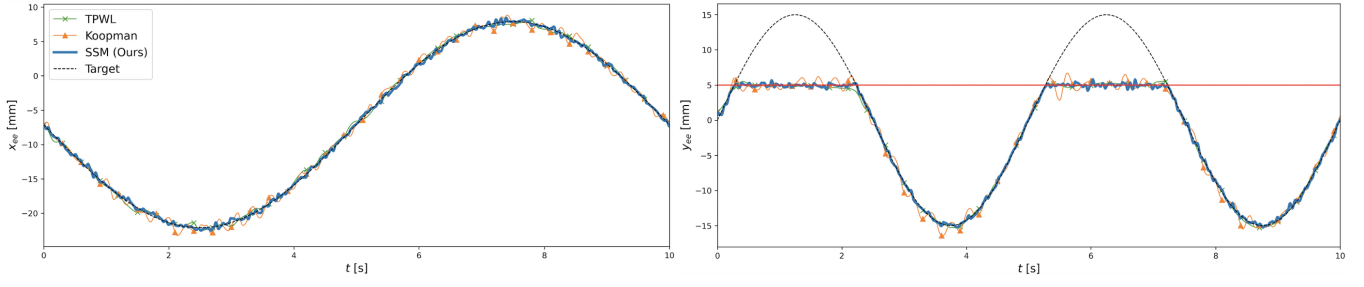


Fig. 3. Simulation results of tracking performance for the quasi-static figure eight (1) with horizon length of $N = 3$. The TPWL controller (green trajectory) uses a rollout horizon $N_r = 3$ and the ROM discretized in time using zero-order hold with sampling time $T_s = 0.1$ s. The Koopman controller (orange trajectory) has a rollout horizon $N_r = 1$ and the controller operates at a sampling time of $T_s = 0.05$ s. Our SSMR-based controller (blue trajectory) has a rollout horizon of $N_r = 2$ and $T_s = 0.03$ s. The dotted black line represents the reference figure 8 trajectory while the red line represent constraints. The MSE (in mm^2) for the TPWL, Koopman, and SSMR approaches are $e_{TPWL} = 0.17$, $e_{Koop} = 0.50$, and $e_{SSM} = 0.12$.

iteration about which we linearize the nonlinear constraints. We can then define the resulting linearized OCP, $(\text{LOCP})_{j+1}$, as follows

$$\begin{aligned} & \underset{\mathbf{u}_{1:N-1}}{\text{minimize}} \quad \|\delta \mathbf{z}_N\|_{\mathbf{Q}_f}^2 + \sum_{k=1}^{N-1} \left(\|\delta \mathbf{z}_k\|_{\mathbf{Q}}^2 + \|\mathbf{u}_k\|_{\mathbf{R}}^2 \right) \\ & \text{subject to} \quad \mathbf{x}_1 = \mathbf{V}^\top (\mathbf{y}_1 - \mathbf{y}_{\text{eq}}) \\ & \quad \mathbf{x}_{k+1} = \mathbf{A}_k^j \mathbf{x}_k + \epsilon \mathbf{B}_r \mathbf{u}_k + \mathbf{d}_k^j, \quad \forall k \in \{1, \dots, N\}, \\ & \quad \mathbf{z}_k = \mathbf{H}_k^j \mathbf{x}_k + \mathbf{c}_k^j, \quad \forall k \in \{1, \dots, N\}, \end{aligned} \quad (11)$$

where $\mathbf{u}_k \in \mathcal{U}$ and $\mathbf{z}_k \in \mathcal{Z}$ are the control and performance constraints, respectively. The terms $\mathbf{A}_k^j \in \mathbb{R}^{n \times n}$ and $\mathbf{H}_k^j \in \mathbb{R}^{o \times n}$ represent Jacobians of the dynamics and the observation map, respectively, while $\mathbf{d}_k^j \in \mathbb{R}^n$ and $\mathbf{c}_k^j \in \mathbb{R}^o$ are the accompanying residuals defined as

$$\begin{aligned} \mathbf{A}_k^j &:= \left. \frac{\partial \mathbf{r}_d}{\partial \mathbf{x}_k} \right|_{\mathbf{x}_k = \mathbf{x}_k^j, \mathbf{u}_k = \mathbf{u}_k^j}, \quad \mathbf{d}_k^j := \mathbf{r}_d(\mathbf{x}_k^j, \mathbf{u}_k^j) - \mathbf{A}_k^j \mathbf{x}_k^j - \mathbf{B}_r \mathbf{u}_k^j, \\ \mathbf{H}_k^j &:= \left. \frac{\partial \mathbf{w}}{\partial \mathbf{x}_k} \right|_{\mathbf{x}_k = \mathbf{x}_k^j, \mathbf{u}_k = \mathbf{u}_k^j}, \quad \mathbf{c}_k^j := \mathbf{C} \mathbf{w}(\mathbf{x}_k^j, \mathbf{u}_k^j) - \mathbf{H}_k^j \mathbf{x}_k^j, \end{aligned} \quad (12)$$

where $\mathbf{r}_d: \mathbb{R}^n \rightarrow \mathbb{R}^n$ represents the time-discretized function of \mathbf{r} . A sequence of $(\text{LOCP})_j$ are solved until convergence i.e., $\|\mathbf{x}^{j+1} - \mathbf{x}^j\|_2 < \varepsilon$ for arbitrarily small ε .

Solving (12) requires each $(\text{LOCP})_j$ to be feasible, which is always possible with the introduction of *virtual dynamics*, as detailed in [20]. Additionally, since linearization provides a good approximation to the nonlinear dynamics only in a small neighborhood around the nominal trajectory, we use *trust regions* to ensure smooth convergence. We implement a modified version of [21] to solve the formulated SCP and treat the constraints on the performance variables as soft constraints.

We solve the finite-horizon problem in a receding horizon fashion, where each receding horizon subproblem involves solving the (LOCP) . This gives an optimal reduced-order model trajectory $(\bar{\mathbf{x}}^*, \mathbf{u}^*) = (\{\mathbf{x}_k^*\}_{k=1}^N, \{\mathbf{u}_k^*\}_{k=1}^{N-1})$ approximating the solution to OCP (3) over an arbitrarily long, finite horizon.

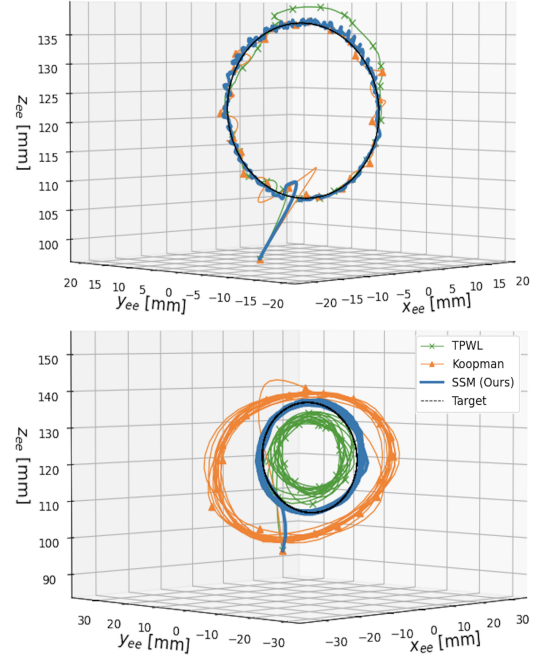


Fig. 4. Top figure shows simulation results of tracking performance for the quasi-static circle (2) while the bottom figure shows results for the near-resonance circle (3) with horizon length of $N = 3$. The controller parameters for each approach are set similarly to those reported in Figure 3. The quasi-static circle MSEs (in mm^2) are $e_{TPWL} = 3.35$, $e_{koop} = 0.91$, and $e_{SSM} = 0.53$. The near-resonance circle MSE are $e_{TPWL} = 21.75$, $e_{koop} = 133.6$, and $e_{SSM} = 1.87$.

V. RESULTS

We now compare our proposed SSMR method against the Trajectory Piecewise-Linear (TPWL) approach [22] and Koopman operator-based control approach [13] in simulations of the elastomer “Diamond” robot (shown in Figure 2), as detailed in [22] and [23]. We show that our approach outperforms these baselines while mitigating their drawbacks, namely lack of generalization, lack of robustness to noise, and computational intractability.

We carry out simulations using the finite-element based SOFA framework [25]; the Diamond robot mesh we used for simulation can be found in the *SoftRobots* plugin [26].

TABLE I. The table on the left shows mean squared error (mm^2) for all considered trajectories while the right shows average cumulative QP solve times (in milliseconds) for the SCP algorithm. The Koopman model consists of polynomials up to order 2 over $\mathbf{z} = [x_{ee}, y_{ee}, z_{ee}]^T$ with a single time delay ($d_{\text{koop}} = 66$). The TPWL model parameters are set similarly to the ones reported in [23] ($d_{\text{TPWL}} = 42$). Our SSM model is of cubic order and although it is low-dimensional ($d_{\text{SSM}} = 6$), it outperforms the other approaches in both tracking performance (at low enough time-discretization) and solve time. The QP is solved using Gurobi [24] on a 2 GHz Intel Core i5 processor with 16 GB of RAM.

Figure 8							Circle				Near-Resonance Circle			Average Solve Times (ms)			
		T_s (ms)	10	20	50	100											
							10	20	50	100	10	20	50	10	20	50	100
$N=3$	SSM (Ours)	0.131	0.123	0.227	0.718	0.481	0.342	1.353	4.480	0.893	1.861	32.87	0.85	0.97	0.97	0.92	
	TPWL	0.166	0.149	0.164	0.191	3.996	3.033	3.197	3.216	4.077	3.789	4.472	25.31	26.19	27.75	31.32	
	Koopman EDMD	1.053	1.230	0.500	0.725	2.985	1.806	0.994	2.060	1.864	6.707	135.3	6.08	6.10	5.95	5.92	
$N=5$	SSM (Ours)	0.153	0.136	0.205	0.757	0.466	0.348	1.287	4.561	0.810	1.816	33.43	1.55	1.49	1.62	1.26	
	TPWL	0.160	0.155	0.160	0.196	3.350	3.278	3.265	3.254	3.698	3.900	4.585	52.20	51.23	55.51	58.52	
	Koopman EDMD	1.540	1.286	0.515	0.679	2.919	1.632	0.895	2.119	1.818	7.149	133.6	15.81	16.18	18.01	19.65	

The parameters of our Diamond robot mirror those reported in [23], where $E = 175$ MPa is the Young's modulus, $\nu = 0.45$ is the Poisson ratio, and $\alpha = 2.5, \beta = 0.01$ represent the usual parameters for Rayleigh damping *i.e.*, $C = \alpha\mathbf{M} + \beta\mathbf{K}$. These parameters were chosen to model the dynamic response of our hardware platform.

In this work, we consider control tasks in which the end effector of the robot is made to follow various trajectories. Thus, the performance variable $\mathbf{z} = [x_{ee}, y_{ee}, z_{ee}]^T$ denotes the position of the top of the robot in its workspace. We also introduce additive Gaussian measurement noise to simulate real-world conditions. We consider three control tasks which include following (1) a figure eight in the x-y plane subject to constraints, (2) a circle in the y-z plane, and (3) the same circle but near resonance with the dominant mode of the system.

A. Simulation

Since we are in a simulation environment, we collect full state information as training data *i.e.*, the i -th dataset is $\mathcal{Y}_i = [\mathbf{x}_1^f, \mathbf{x}_2^f, \dots, \mathbf{x}_M^f]^T$. We obtain this data by displacing the robot along 44 different directions and amplitudes in its workspace. We observe state transitions sampled at $T_s = 1$ ms, which is consistent since the highest frequency mode in the SSM has a period of roughly 330 ms. After conducting PCA on our training data, we found that the 3 leading configuration modes (6 modes in phase space) captured more than 95% of the variance in our dataset. Hence, we learn a cubic order, 6-D autonomous SSM parametrization described in (6) and its reduced dynamics (9) using the procedure in Section III. Lastly, we learn the control matrix by randomly sampling controls and then collect the resulting state transitions sampled at 10 ms.

Table I reports the mean-squared error tracking performance and average *cumulative* time to solve the QP for all trajectories at various controller parameters and time discretization of Equation (9). To enable real-time control, we seek control parameters such that the controller sampling time is at least an order of magnitude less than the solve time. Figures 3 and 4 depict simulation results for trajectories (1), (2), and (3) for controller parameters chosen to maximize performance while enabling real-time control.

These results show that our SSM-based MPC scheme outperforms the TPWL and the Koopman approach in tracking performance across all trajectories considered, for small enough time discretization. Thus, our approach exhibits superior generalizability to control tasks as shown in the above figures and tables. Due to the low dimensionality of our learned model, we can solve the SCP iterations quickly and the computational burden grows modestly as the MPC horizon increases. As shown in Table I, the solve times for our approach are magnitudes lower than for the TPWL and Koopman-based methods, giving us more freedom to choose the controller parameters to enable real-time control.

Additionally, the SSMR approach offers several practical advantages over the alternatives. First, our SSM-based model exhibits good closed-loop performance at longer horizons and does not suffer from numerical conditioning issues that plague the Koopman approach. We found that at horizons $N \geq 10$, the Koopman QPs were no longer solvable, which is likely due to ill-condition of the Koopman matrices.

Second, our approach involves only two parameters: the order approximation and dimension of the manifold. Of these two, the dimension of the SSM is a property of the system dynamics, which can be inferred via a frequency analysis of the available data. The polynomial order of the SSM approximation controls the accuracy and the trade-off between generalization and overfitting. The size of the Koopman model grows rapidly with the number of observed states while the dimension of the projection basis for TPWL needs to be fairly large for acceptable closed-loop performance. In contrast, since off-manifold dynamics are sufficiently approximated by those on the SSM for closed-loop control, we can learn models of minimal size and tune the SSM order iteratively to increase model fidelity, as needed. This has considerable practical advantage over learning-based approaches where it is well-known that closed-loop performance is highly sensitive to choice of dictionary features, size, and regularization.

VI. CONCLUSION AND FUTURE WORK

In this work, we proposed a new data-driven approach for constructing control-oriented, reduced models of soft robots on spectral submanifolds. Using our approach, we can construct faithful, predictive, low-dimensional models which can be effectively used for real-time optimal control. We

demonstrated that our SSM-based MPC scheme outperforms the state of the art significantly in both tracking error and computation time.

Hardware experiments are ongoing and their results will be reported in an updated manuscript. We also plan to extend our work to handle configuration-dependent actuation constraints which lead to dynamics with state-affine control. Lastly, we plan to estimate errors arising from SSM approximation *a priori* and derive error bounds for constraint-tightening control schemes in an MPC framework.

ACKNOWLEDGMENT

The authors thank Elisabeth Alora and Matteo Zallio for generating the instructive figures, Florian Mahlknecht for thoughtful discussions and help with initial implementations, and Spencer Richards for his careful review of the manuscript.

REFERENCES

- [1] G. Haller and S. Ponsioen, “Nonlinear normal modes and spectral submanifolds: Existence, uniqueness and use in model reduction,” *Nonlinear Dynamics*, vol. 86, no. 3, pp. 1493–1534, Nov. 2016, ISSN: 1573-269X.
- [2] M. Cenedese, J. Axås, B. Bäuerlein, K. Avila, and G. Haller, “Data-driven modeling and prediction of non-linearizable dynamics via spectral submanifolds,” *Nature Communications*, vol. 13, no. 1, p. 872, Feb. 2022, ISSN: 2041-1723.
- [3] D. C. Rucker, R. J. Webster III, G. S. Chirikjian, and N. J. Cowan, “Equilibrium conformations of concentric-tube continuum robots,” *The International journal of robotics research*, vol. 29, no. 10, pp. 1263–1280, 2010.
- [4] G. S. Chirikjian, “Hyper-redundant manipulator dynamics: A continuum approximation,” *Advanced Robotics*, vol. 9, no. 3, pp. 217–243, 1994.
- [5] J. Jung, R. S. Penning, N. J. Ferrier, and M. R. Zinn, “A modeling approach for continuum robotic manipulators: Effects of nonlinear internal device friction,” in *2011 IEEE/RSJ International Conference on Intelligent Robots and Systems*, IEEE, 2011, pp. 5139–5146.
- [6] M. Thieffry, A. Kruszewski, C. Duriez, and T.-M. Guerra, “Control design for soft robots based on reduced-order model,” *IEEE Robotics and Automation Letters*, vol. 4, no. 1, pp. 25–32, 2018.
- [7] R. K. Katzschmann, M. Thieffry, O. Gourey, A. Kruszewski, T.-M. Guerra, C. Duriez, and D. Rus, “Dynamically closed-loop controlled soft robotic arm using a reduced order finite element model with state observer,” in *2019 2nd IEEE international conference on soft robotics (RoboSoft)*, IEEE, 2019, pp. 717–724.
- [8] C. Della Santina, R. K. Katzschmann, A. Bicchi, and D. Rus, “Model-based dynamic feedback control of a planar soft robot: Trajectory tracking and interaction with the environment,” *The International Journal of Robotics Research*, vol. 39, no. 4, pp. 490–513, 2020.
- [9] S. Tonkens, J. Lorenzetti, and M. Pavone, “Soft robot optimal control via reduced order finite element models,” in *Proc. IEEE Conf. on Robotics and Automation*, 2021.
- [10] O. Gourey and C. Duriez, “Fast, generic, and reliable control and simulation of soft robots using model order reduction,” *IEEE Transactions on Robotics*, vol. 34, no. 6, pp. 1565–1576, 2018.
- [11] T. G. Thuruthel, E. Falotico, F. Renda, and C. Laschi, “Model-based reinforcement learning for closed-loop dynamic control of soft robotic manipulators,” *IEEE Transactions on Robotics*, vol. 35, no. 1, pp. 124–134, 2018.
- [12] D. Bruder, C. D. Remy, and R. Vasudevan, “Nonlinear system identification of soft robot dynamics using koopman operator theory,” in *2019 International Conference on Robotics and Automation (ICRA)*, IEEE, 2019, pp. 6244–6250.
- [13] D. Bruder, B. Gillespie, C. D. Remy, and R. Vasudevan, “Modeling and control of soft robots using the koopman operator and model predictive control,” *arXiv preprint arXiv:1902.02827*, 2019.
- [14] S. L. Brunton, B. W. Brunton, J. L. Proctor, and J. N. Kutz, “Koopman invariant subspaces and finite linear representations of nonlinear dynamical systems for control,” *PloS one*, vol. 11, no. 2, e0150171, 2016.
- [15] C. Della Santina, C. Duriez, and D. Rus, “Model based control of soft robots: A survey of the state of the art and open challenges,” *arXiv preprint arXiv:2110.01358*, 2021.
- [16] M. Cenedese, J. Axås, H. Yang, M. Eriten, and G. Haller, “Data-driven nonlinear model reduction to spectral submanifolds in mechanical systems,” *Philosophical Transactions of the Royal Society A*, vol. 380, no. 2229, p. 20210194, 2022.
- [17] J. Axås, M. Cenedese, and G. Haller, “Fast data-driven model reduction for nonlinear dynamical systems,” *arXiv preprint arXiv:2204.14169*, 2022.
- [18] J. L. Proctor, S. L. Brunton, and J. N. Kutz, “Dynamic mode decomposition with control,” *SIAM Journal on Applied Dynamical Systems*, vol. 15, no. 1, pp. 142–161, 2016.
- [19] D. Malyuta, T. P. Reynolds, M. Szmuk, T. Lew, R. Bonalli, M. Pavone, and B. Acikmese, “Convex optimization for trajectory generation,” *IEEE Control Systems Magazine*, 2022, In Press.
- [20] Y. Mao, M. Szmuk, and B. Açikmeşe, “Successive convexification of non-convex optimal control problems and its convergence properties,” in *2016 IEEE 55th Conference on Decision and Control (CDC)*, IEEE, 2016, pp. 3636–3641.
- [21] R. Bonalli, A. Bylard, A. Cauligi, T. Lew, and M. Pavone, “Trajectory optimization on manifolds: A theoretically-guaranteed embedded sequential convex programming approach,” in *Robotics: Science and Systems*, 2019.

- [22] S. Tonkens, J. Lorenzetti, and M. Pavone, *Soft robot optimal control via reduced order finite element models*, 2021. arXiv: 2011.02092 [cs.R0].
- [23] J. Lorenzetti, “Reduced order model predictive control of high-dimensional systems,” Ph.D. dissertation, Stanford University, Dept. of Aeronautics and Astronautics, Stanford, California, Aug. 2021.
- [24] Gurobi Optimization, LLC, *Gurobi Optimizer Reference Manual*, 2022.
- [25] J. Allard, S. Cotin, F. Faure, P.-J. Bessoussan, F. Poyer, C. Duriez, H. Delingette, and L. Grisoni, “Sofa-an open source framework for medical simulation,” in *MMVR 15-Medicine Meets Virtual Reality*, IOP Press, vol. 125, 2007, pp. 13–18.
- [26] E. Coevoet, T. Morales-Bieze, F. Largilliere, Z. Zhang, M. Thieffry, M. Sanz-Lopez, B. Carrez, D. Marchal, O. Gourey, J. Dequidt, *et al.*, “Software toolkit for modeling, simulation, and control of soft robots,” *Advanced Robotics*, vol. 31, no. 22, pp. 1208–1224, 2017.